Deliverable D3.2

Parameterisations delivered to WP6 from WP3

27.08.2025/version1.0

OceanICU was funded by the European Union under grant agreement no. 101083922 and UK Research and Innovation (UKRI) under the UK government's Horizon Europe funding guarantee [grant number 10054454, 1006367, 10064020, 10059241, 10079684, 10059012, 10048179]. Views and opinions expressed are however those of the author(s) only and do not necessarily reflect those of the European Union or European Research Executive Agency. Neither the European Union nor the granting authority can be held responsible for them.

About this document

Title	D3.2, Parameterisations delivered to WP6 from WP3
Work Package	[WP3, Impacts of Abiotic Climate Stressors on the Biological Carbon Pump]
Lead Partner	Jan Taucher (GEOMAR)
Lead Author (Org)	Jan Taucher (GEOMAR)
Contributing Author(s)	-
Reviewers	Alex Poulton (HW), Richard Sanders (NORCE)
Due Date	31.08.2025, M34
Submission Date	27.08.2025
Version	**1.0**

Dissemination Level

x	PU: Public – fully open (automatically posted online)
	SEN: Sensitive – limited under the conditions of the Grant Agreement

OceanICU: Improving Carbon Understanding is a Research and Innovation action (RIA) funded by the Horizon Europe Work programme topics addressed: HORIZON-CL6-2022-CLIMATE-01-02. Start date: 01 November 2022. End date: 31 October 2027.

This work was funded by the European Union under grant agreement no. 101083922 (OceanICU) and UK Research and Innovation (UKRI) under the UK government's Horizon Europe funding guarantee [grant number 10054454, 10063673, 10064020, 10059241, 10079684, 10059012, 10048179]. Views and opinions expressed are however those of the author(s) only and do not necessarily reflect those of the European Union or European Research Executive Agency. Neither the European Union nor the granting authority can be held responsible for them.

Contents

1. Key messages for the Ocean ICU stakeholders 4
2. Abstract 4
3. Work carried out 4
4. Main results achieved 17
5. Contribution to the overall objectives and relevant (KPIs) 17
6. Impact and progress beyond state of the art 17
7. Lessons learnt and links built 17
8. References 18

Key messages for the Ocean ICU stakeholders

Abstract

Within the biological carbon pump (BCP), marine particles transport carbon to the deep ocean. However, historically it was a very time-consuming effort to study particle transport over the entire water column in detail. Now, in-situ imaging devices such as the Underwater Vision Profiler (UVP5 & 6) allow for analysis of particle distribution in high spatial resolution.
In our work, we use a large published UVP dataset with global information on particle size, abundance, distribution and biovolume which we match with environmental data from several other data sources.
The specific goal of this work was to assess the influence of temperature, oxygen and pH on flux attenuation and biological pump efficiency, and based on this, derive mathematical parameterizations of the control of these environmental drivers for testing and application in models.
Therefore, we use three traditionally used organic flux attenuation measures; Martin's b, the remineralization depth, and the transfer efficiency. However, we do not find a simple relationship between environmental drivers and attenuation metrics in this data set.
Due to the lack of any statistically significant relationship, no mathematical relationships for sensitivities or new parameterizations for implementation in models can be developed. To uncover more complex patterns, we apply unsupervised clustering to the environmental data and relate the resulting clusters to the attenuation metrics, to reveal geographic patterns of environmental influence.
Additionally, we observe that many vertical particle flux profiles deviate from traditional power law attenuation curve shapes, often featuring intermediate particle maxima (IPM), making metrics like Martin b less applicable. We map the global distribution of IPM, categorize them by intensity, and find they are widespread, particularly abundant in coastal regions and around the equator. We also assess the influence of IPMs on widely used metrics for BCP metrics.

Work carried out

The goal of work package (WP) 3.2 is to quantify the impact of the environmental drivers temperature (T), oxygen (O), and pH, on the biological carbon pump (BCP).

We focus on vertical particle fluxes (i.e. the gravitational part of the BCP), and particularly on flux attenuation with depth, which determines the efficiency of the BCP.

Analysis of the global UVP5 dataset

Within WP 3.2.1 the focus is set on the influence of climate stressors (T, O, and pH) on vertical particle fluxes using the global in situ imaging dataset from the Underwater Vision Profiler (UVP), which contains almost 9000 profiles that were collected between 2008 and 2020 (Kiko et al., 2022).

For WP 3.2.2 the goal is to estimate the quantitative relationship between the above mentioned climate stressors and the stoichiometry (C:N:Si:P) of vertical particle fluxes to examine element-specific length scales. This is done by using sediment trap data from existing data bases such as Mouw et al., 2016.

Work on the project started on 01/01/2024 and has so far focused mainly on WP 3.2.1.

The UVP is a vertically profiling underwater camera system that detects particles in the size range from approx. 100 µm to several cm (Kiko et al., 2022). For each particle, information on size, area, shape etc. are collected. Collected data are then processes to particle counts in different size classes. This data can be further processed to convert to biovolume, as well as carbon flux (using previously published parameterizations for size-dependent carbon content and size-dependent sinking velocity).

Initially, to get a first impression, subsets of the UVP data were inspected visually and a data formatting pipeline was constructed that would allow to include or exclude specific particle size classes or variables and compute newly calculated metrics on the input data. This pipeline was continuously tweaked and improved. Then environmental data were matched to the same 3D grid using data from WOA for temperature and oxygen (Garcia et al., 2024; Locarnini et al., 2024) and for pH first GLODAP (Key et al., 2015; Olsen et al., 2016) and later Mercator global re-analysis model data (European Union-Copernicus Marine Service, 2018) as GLODAP does not provide the temporal range necessary to cover the majority of UVP data points.

Several widely used measures for flux attenuation and biological pump efficiency were calculated using the total particle biovolume (integrated across size classes) derived from the UVP data.

Influence of environmental drivers on BCP metrics

In a first step, we applied a simple linear model between surface and deep particle biovolume, to get a first impression of the effects of environmental drivers. Temperature was mainly used as an environmental driver since it was thought to have the clearest effect and the most reliable data. However, with this approach, no relationship between temperature and attenuation intensity was found.

(I) Remineralization length scale was calculated as the depth at which 63% attenuation from the flux at euphotic zone has occurred. This required the inclusion of euphotic zone depth data which was taken from Bianchi & Clements, 2023. Initially, this remineralization depth was calculated from biovolume but was later changed to Flux (mg C m^2), which was calculated using the Clements et al., 2023 function. The remineralization depths were found to be sensitive to noise in the data. Therefore, the data were smoothed with a lowess algorithm after a few alternatives were considered and testing was done on the impact of the smoothing on remineralization depths. Additionally, a simple algorithm was written to remove the nepheloid layer based on bathymetry data retrieved from the GEBCO database (GEBCO Bathymetric Compilation Group 2023). Afterwards, analysis of the remineralization depth was repeated but no significant relationship with environmental drivers was found (Figure 2, 3). The relationship was also reviewed for individual biogeochemical provinces (Longhurst, 2007; Reygondeau et al., 2013), yet there was no relationship found (Figure 4, 5).

(II) Transfer efficiency (T_{eff}) was calculated as the difference in particle flux between euphotic zone depth and 1000dbar (in a later step also 2000dbar), respectively. There was no significant relationship with any environmental driver (Figure 3).

(III) The classical “Martin curve” model (power law) was fit to flux over depth and goodness of fit was estimated using R^2 of the original data against the fit data and correlation (Figure 2). The Martin b coefficient – describing the steepness of decline in flux – was used to estimate flux attenuation and remineralization across the profiles. Profiles with a R^2 above 0.5 were used to look for a relationship with environmental parameters. However, there was again no clear relationship found.

Notably, during the initial visual inspection, we found that a large portion of the flux profiles do not follow the traditionally expected shape of a decreasing power law curve (Figure 1) (Martin et al., 1987). Transfer efficiency and remineralization depth are simple metrics that are independent of the shape of the flux profile, and were therefore

in most cases insensitive to diverging profile shapes. However, for the fitting of the Martin curve it meant that flux attenuation could only be computed for a reduced portion of profiles, which followed the power law shape close enough. For that, we determined that the goodness of fit should be at least $R^2 > 0.5$. Therefore, plans were made to group the profiles by shape and thus be able to easily sort out power law and non-power law shaped profiles. Indeed, a large portion of profiles show the existence of a second maximum in the twilight zone (intermediate particle maxima; IPM), which could be one factor obscuring a possible relationship between environmental drivers and flux attenuation (see section 3, Outlook).

Besides the issues with Martin curve fitting to non-conforming profiles, the absence of a relationship can also have other reasons. Among those reasons are a lack of spatiotemporal coverage in some ocean regions and seasons, uncertainties related to the UVP system in itself and the steps taken to format the data and calculate the flux, and the variability of natural parameters. The latter being the main aspect thought to mask potential effects of T, O and pH. Therefore, the inclusion of chlorophyll-*a* and net primary production is being worked on currently to estimate their influence on flux in comparison to the previously tested drivers. These will then also be included in a multivariate statistical analysis.

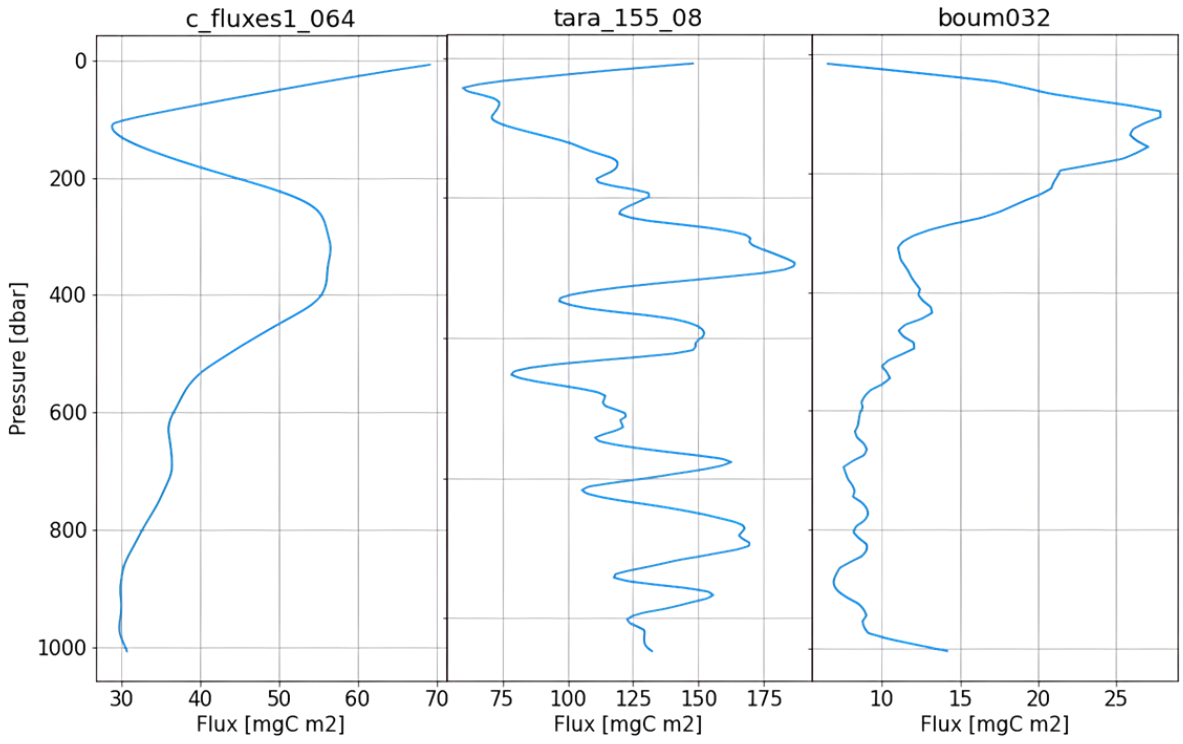

Figure 1 | Example profiles showing different types of particle flux curves in the global UVP dataset.

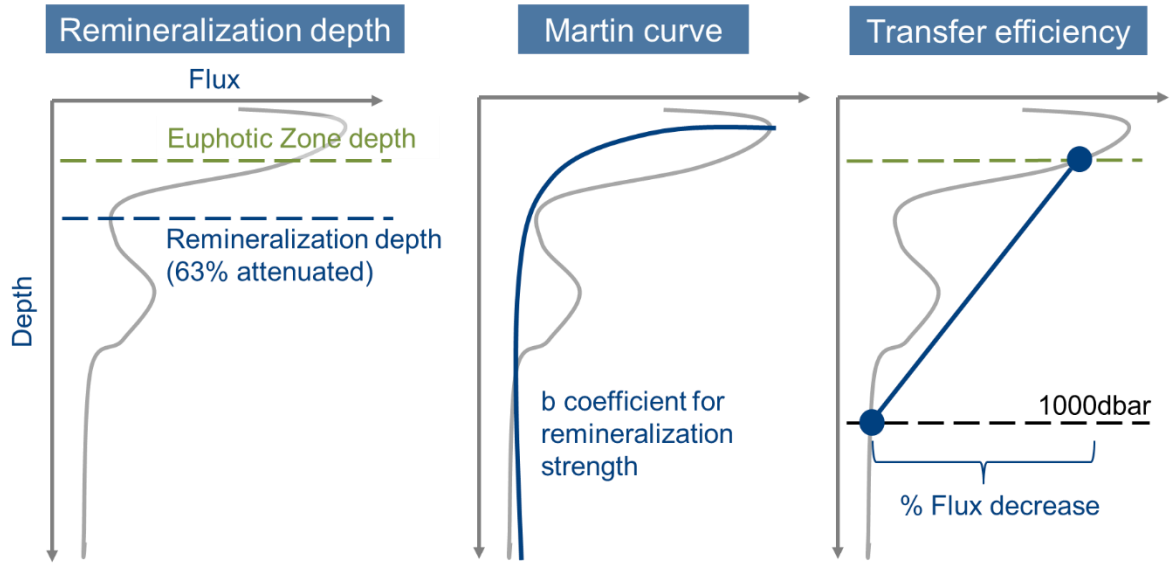

Figure 2 | Metrics calculated to estimate attenuation of flux over depth in the UVP data. From left to right: Remineralization depth is defined as the depth at which 63% of flux at euphotic zone depth are attenuated, Martin curve is a power law fit to the flux data where then the b coefficient is directly linked to the remineralization strength and transfer efficiency is a simple measure where the ratio of flux from euphotic zone depth to 100dbar is calculated.

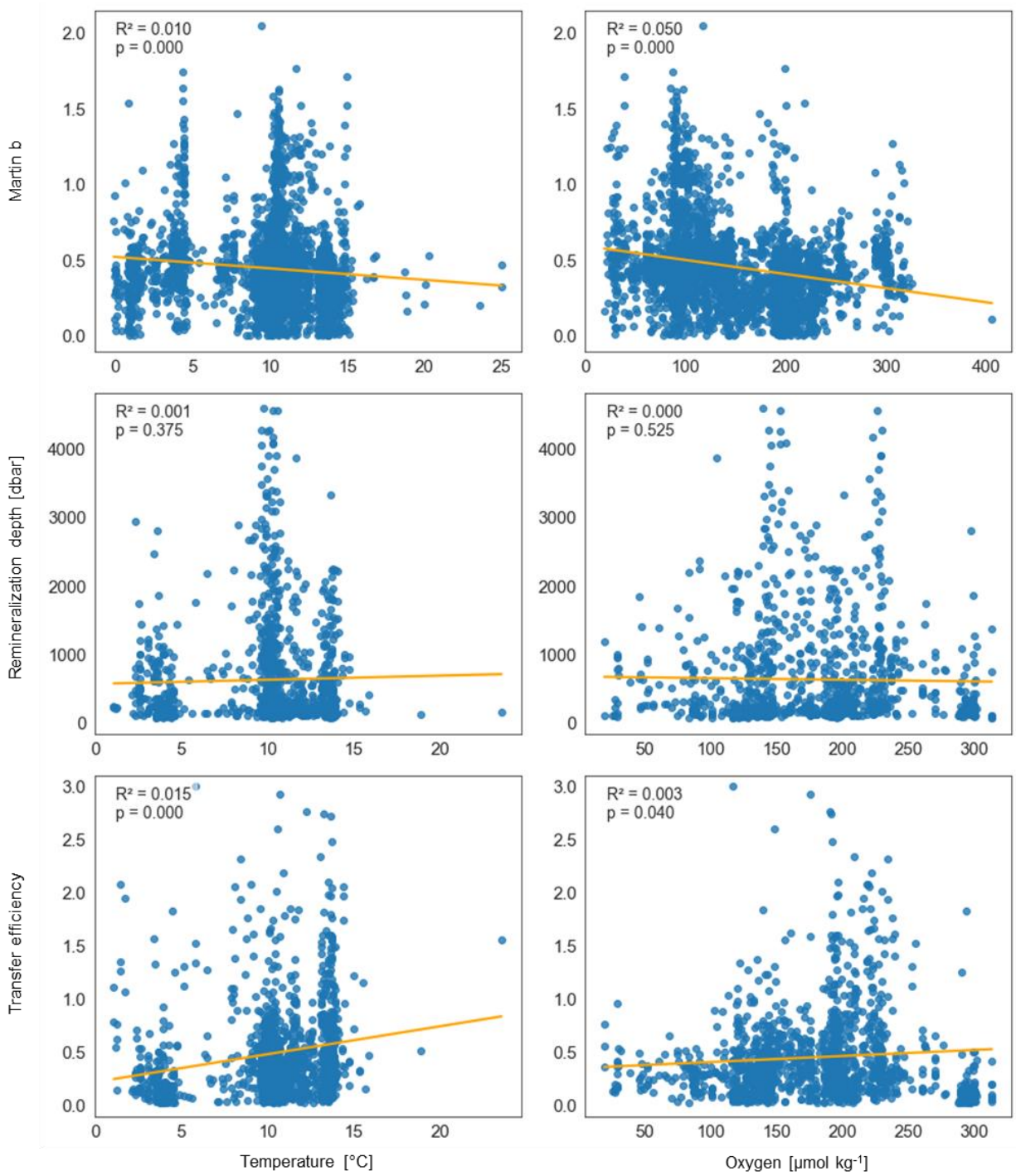

Figure 3 | Linear regressions between environmental parameters and Martin b, remineralization depth [dbar], and T_{eff} (Z_{eu} to 1000dbar). Left column shows relationship to temperature and right column with oxygen. Both environmental drivers are calculated as an average of values between 17 and 500dbar in 50dbar steps (17dbar, 50dbar, 100dbar, 150dbar, etc.). 12 outliers in the T_{eff} plots between 3 and 10 were cut out.

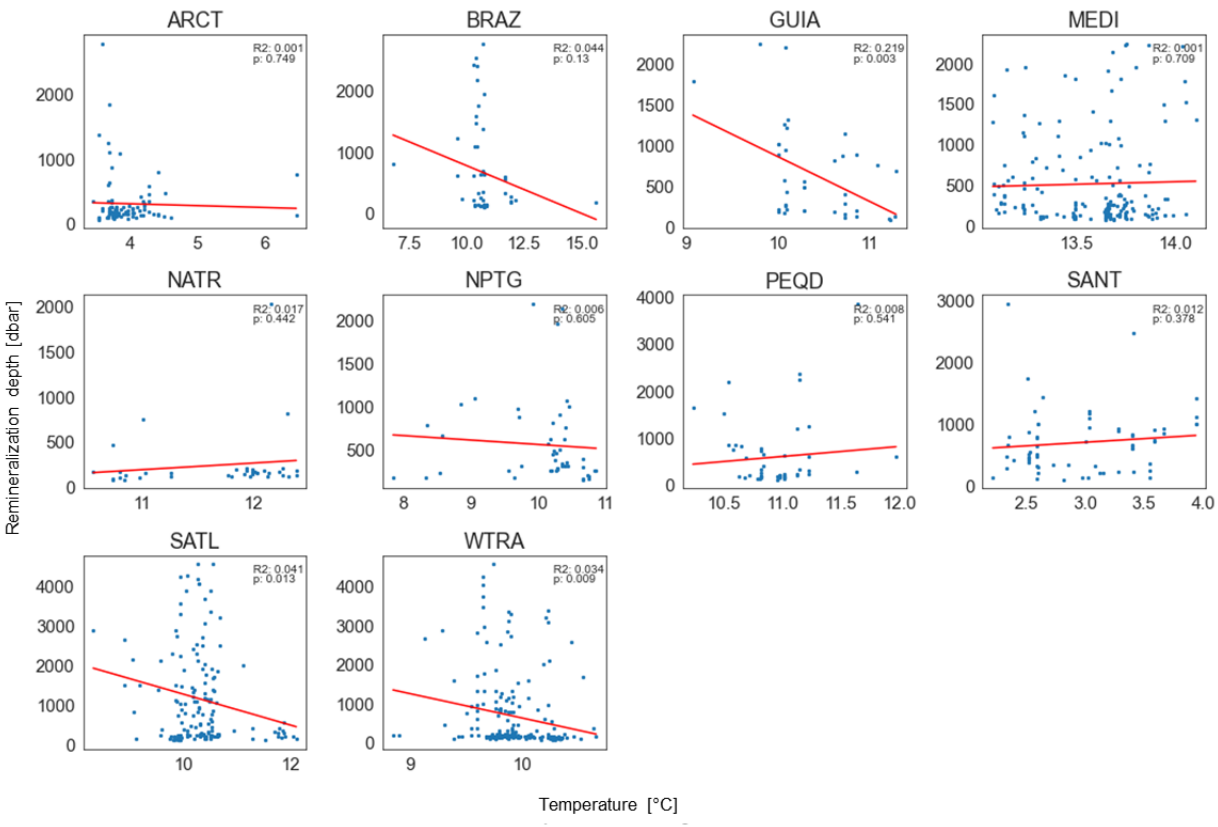

Figure 4 | Linear regressions between remineralization depth and temperature average per Longhurst biogeochemical region. Only regions with more than 30 profiles were considered, with each profile having to be at least 500dbar deep. Longhurst regions: ARCT: Atlantic Arctic; BRAZ: Brazilian current coast; GUIA: Guianas coast; MEDI: Mediterranean Sea; NATR: North Atlantic tropical gyral; NPTG: North Pacific tropical gyre; PEQD: Pacific equatorial divergence; SANT: Subantarctic water ring; SATL: South Atlantic gyral; WTRA: Western tropical Atlantic

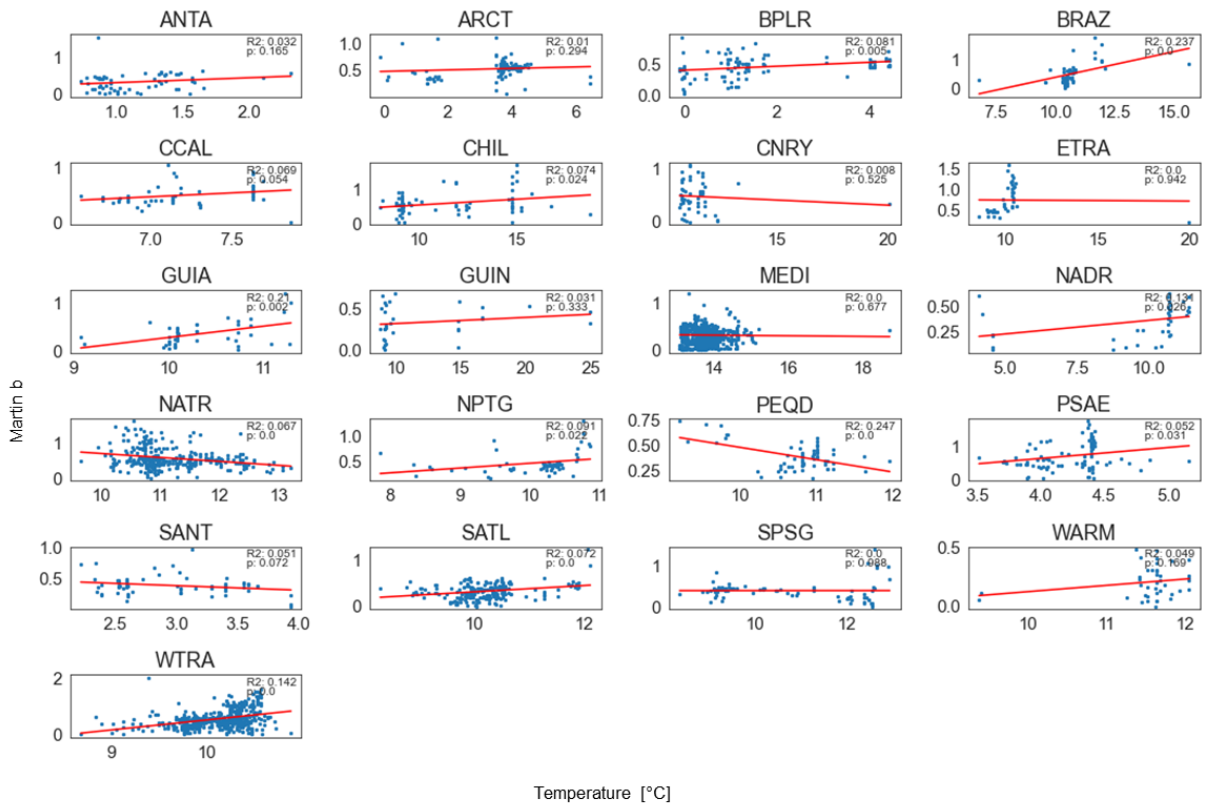

Figure 5 | Linear regressions between the b coefficient of Martin curve fit to the flux profiles and the temperature average per Longhurst region. Only regions with more than 30 profiles were considered. Longhurst regions: ANTA: Antarctic; ARCT: Atlantic Arctic; BPLR: Boreal polar; BRAZ: Brazilian current coast; CCAL: Coastal Californian current; CHIL: Chile-Peru current coastal; CNRY: Canary coast current; ETRA: Eastern tropical Atlantic; GUIA: Guianas coast; MEDI: Mediterranean Sea; NADR: North Atlantic Drift; NATR: North Atlantic tropical gyral; NPTG: North Pacific tropical gyre; PEQD: Pacific equatorial divergence; PSAE: Eastern Pacific subarctic gyres; SANT: Subantarctic water ring; SATL: South Atlantic gyral; SPSG: South Pacific subtropical gyre; WARM: Western Pacific warm pool; WTRA: Western tropical Atlantic

Handling “non-typical” vertical flux profiles

In order to address the issues of different profile shapes, we started developing a clustering pipeline for the variety of profiles shapes to be able to quickly sort them into different categories. This would allow easily sort out profiles that adhere to the Martin curve shape or those that exhibit an intermediate particle maximum (IPM), i.e. an increase in particle number and flux at midwater depths, which is frequently observed and likely caused by diel vertical migration of zooplankton. The initial clustering approach was to use a dimension reduction algorithm such as PCA, t-SNE or UMAP and then a clustering algorithm such as KMeans or GMM to divide the dimension

reduced profiles into clusters of equal shape. Two more approaches were tested afterwards. The first being variance-based binning along the pressure axis to find groups based on similarity of biovolume/flux within the defined bins and the second being wide clustering and then manually reassembling the clusters into the minimal amount possible. The second approach yielded quite good results yet was ultimately not further pursued as it shifted too far from the original goal.

Towards the end of the 2024, we established a collaboration with Daniel Clements to share insights of ongoing efforts in using the UVP global data set. Daniel Clements used a machine learning approach to compute a global 3D flux product, using the UVP data as a training set and a new function to calculate flux that factors in changing sinking speed over depth. The data set was used to estimate whether an updated flux function and a global machine learning approach reveal a relationship between environmental drivers and flux attenuation. However, comparing the data proved to be difficult due to several of the formatting steps differing and since in the product itself there was also no relationship found, work around the data product was halted.

Intermediate particle maxima and their influence on BCP metrics

In 2025 the direction of this task in WP3 was slightly shifted as the original approaches for quantifying flux attenuation did not find significant relationships with any of the environmental drivers. One hypothesis was, that this was also due to the high number of “non-Martin-curve” profiles, and thereby possibly the influence of zooplankton vertical migration.

Many of the finely spatially resolved profiles do not follow a power law curve as we at least partially expected. A large number of deep profiles (≥1000dbar max. depth) have an intermediate particle maximum (IPM) which vary in intensity and vertical scale. The goal of this analysis is to assess how common IPMs are, how relevant they are (e.g. how strong is their influence on the vertical flux), and to assess their spatial distribution. Therefore, we developed an algorithm that detects IPM to analyze whether they are affecting the fit of the Martin curve and thus skew the potential relationship to environmental drivers (Figure 6). The algorithm discriminates between surface (<150dbar) and deep (>150dbar) values. Per definition, an IPM cannot be found in the surface layer but is also discarded if it is found within 900-1000dbar to avoid potential influences of resuspension at the sea floor.

The algorithm detects all curve peaks above a set prominence threshold. Prominence describes the distance of a peak to the nearest neighbouring valley. This threshold is set very low (0.1 mgC m^2) to find even the smallest curve bumps. On top of that three other metrics are calculated for each peak: the relative height to the surface peak ($IPMsurf_{ratio}$) (defined as the maximum flux value between 0 - 150dbar), the relative ($IPMmin_{ratio}$) and the absolute ($IPMmin_{abs}$) height differential to the preceding flux minimum (the flux minimum above each individual peak, respectively). The IPM with the highest $IPMmin_{abs}$ per profile is considered the main IPM for that profile and for all diagnostics and analyses. The detected peaks are classified into five intensity levels based on the $IPMmin_{abs}$. Intensity levels are divided logarithmically to account for the high abundance of low peaks into 0.1-1-10-100-1,000-10,000 bins. (Fig 6)

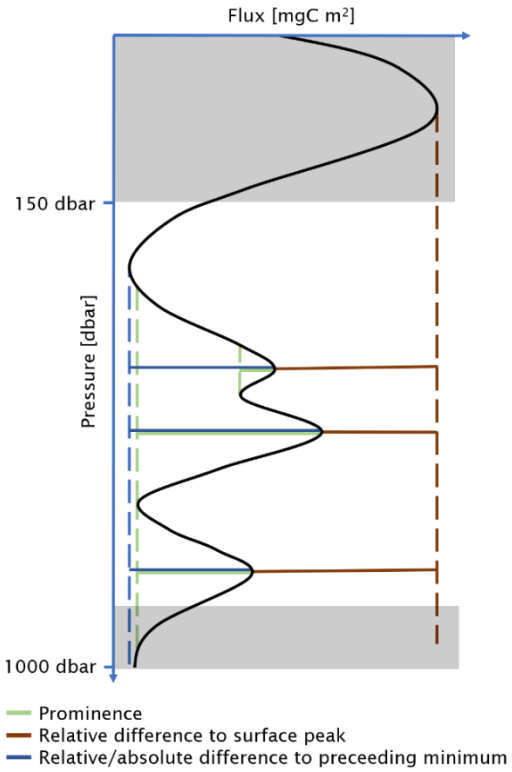

Figure 6 | Schematic of the different metrics derived from the peak finding algorithm. Prominence (green) describes the offset towards the higher of the neighbouring contour lines, effectively showing how much a peak stands out. Relative difference to surface peak (red) is the ratio between intermediate particle maximum (IPM) and the maximum flux at the surface (<150dbar) ($IPMsurf_{ratio}$). Relative and absolute difference to preceeding minimum (blue) reference the minimum above and describe the relative or absolute difference towards the individual peak ($IPMmin_{ratio/abs}$). If multiple peaks are detected the highest one is considered the IPM

Preliminary results reveal that IPMs are a common feature in the ocean. This contradicts the classical paradigm of gravitational flux, i.e. that it is monotonically decreasing from the surface to the deep ocean (and following a power law “Martin’s” curve). While their relative magnitude is relatively low in most cases, there is also a notable portion of profiles where IPMs reach at least half of the flux from the euphotic zone or even more (Figure 7). This indicates that IPMs need to be considered in assessments of vertical flux profiles and studies of biological pump efficiency.

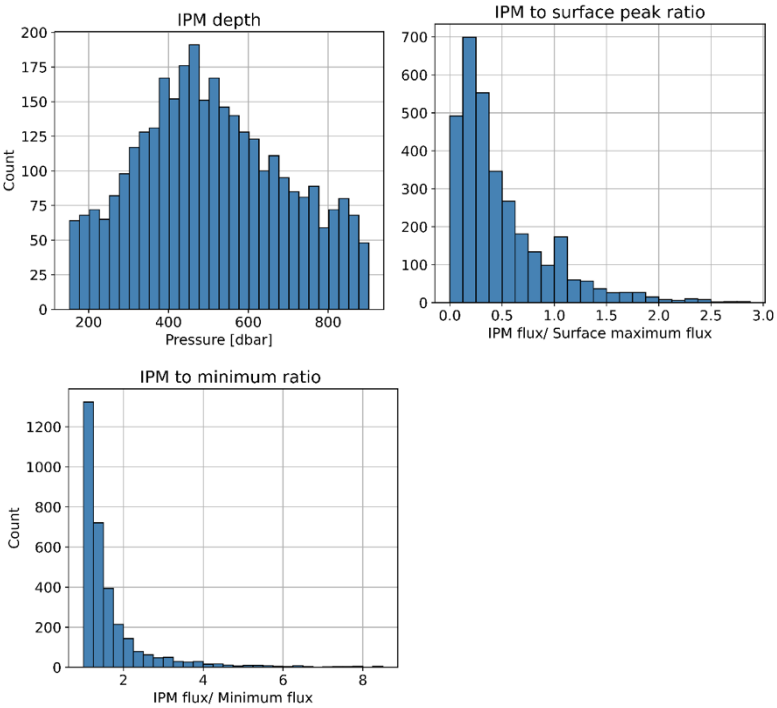

Figure 7 | Intermediate particle maxima (IPM) analytics histograms showing the different metrics calculated. IPM depth describes the depth at which the flux peak with the highest prominence per profile is found (left). The IPM to surface peak ratio describes the relative magnitude of flux in the IPM compared to the maximum flux within the euphotic zone (middle). The IPM to minimum ratio describes the relative increase in flux compared to minimum flux above, i.e. in the depths between the lower end of the euphotic zone and the detected IPM (right).

Globally, IPM intensities are not uniformly distributed. Low and Medium IPM profiles are mirroring the general distribution of the UVP data overall. Most profiles in these two classes are located in the Western Mediterranean and around the Atlantic equatorial region. High IPM profiles are also most abundant in the Western

Mediterranean, however, the overall distribution is different. The majority of High IPM profiles are located in coastal areas, with only a few profiles in the open ocean regions, e.g. in the Southern Ocean, south of the Indian Ocean and the Northern Atlantic south of Greenland. For the coastal profiles, most High IPM were found off West Africa and in the Peruvian/ Chilean upwelling system. Very High IPM profiles are rare and like the High profiles almost exclusively occurred in coastal regions (Fig 8).

Overall, the same patterns are present when looking at microscopic particle abundance (0.1 to 0.512mm) instead of flux for IPM detection. Only for the Very High IPM profiles are there discrepancies in the distribution, though they are equally rare compared to the flux calculated IPM.

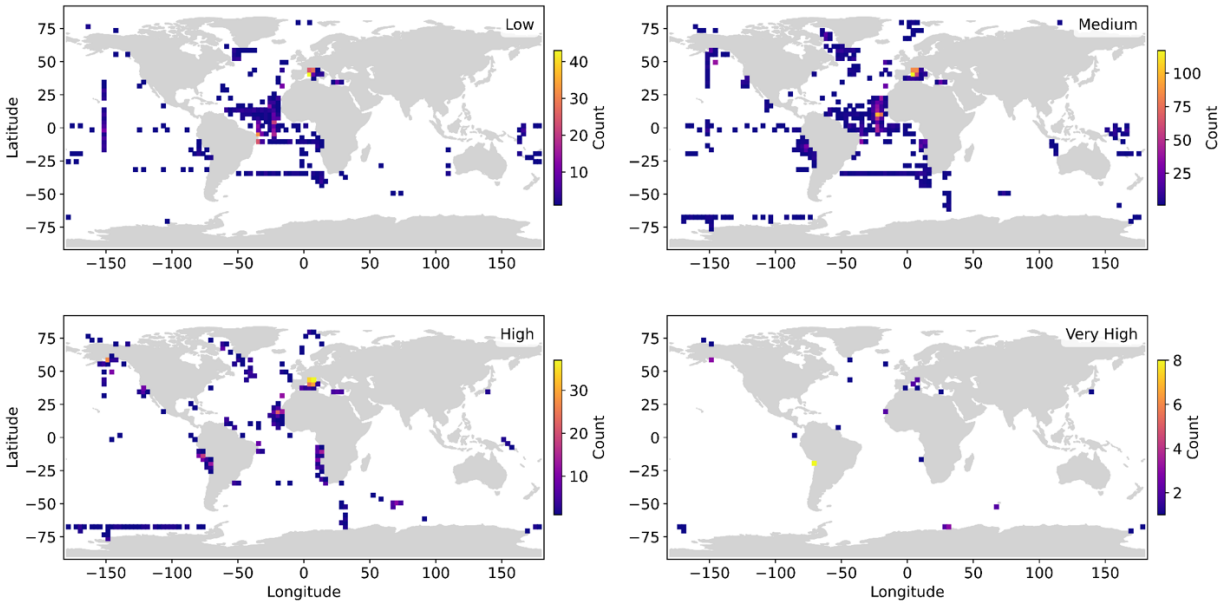

Figure 8 | Distribution of different intermediate particle maxima (IPM) intensity groups. The division is based on logarithmic brackets of the absolute difference (given in mgC m^{-2} d^{-1} of the respective IPM flux to minimum flux above $IPMmin_{abs}$. Brackets are: Low (0.1-1), Medium (1-10), High (10-100), Very High (100-1000), and Extreme (>1000). Extreme was only found once using this method, and is thus not displayed.

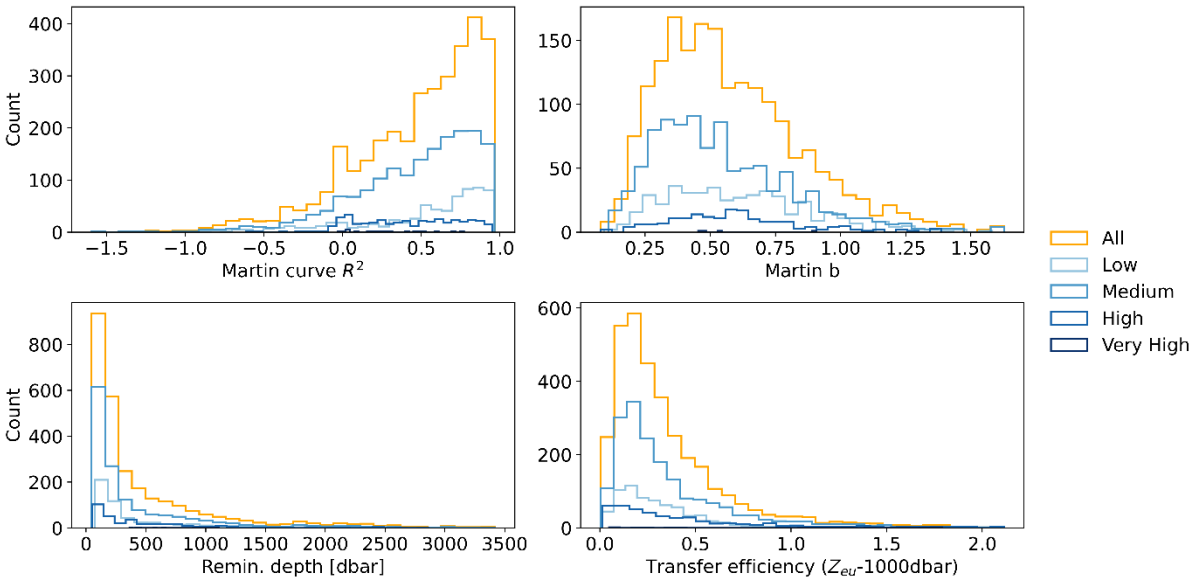

Figure 9 | Distribution of attenuation metrics Martin b, remineralization depth, and transfer efficiency and R^2 of Martin curves grouped by IPM intensity classes. Martin b values included are R^2>0.5. IPM classes are based on difference between minimum flux and IPM flux with logarithmic thresholds (0.1-1-10-100-1000->1000). Included are all profiles that are at least 1000dbar deep (n=4048). The data in the plot represent the 99 percentile of the respective variable to reduce skew through individual outliers.

The presence of IPM affects the overall distribution of the attenuation metrics used in this study (Fig 9). While the distribution of attenuation metrics is mostly the same in low and medium IPM profiles, high IPM profiles display a different distribution for Martin b and T_{eff}. With Martin b values not showing a peak at around 0.3-0.4 like the main distribution but rather being more continuously distributed with a small peak at around 0.6. Median Martin b is between 0.5 and 0.6 for all IPM classes and all profiles. Contrary to the low and medium intensity IPM profiles, high IPM profiles also do not increase in abundance towards high Martin curve R^2. The median fit of high IPM profiles is lower (0.41) than for profiles with low (0.66) or medium (0.55) IPM.

The median T_{eff} value is highest for profiles with a high IPM (0.33), whereas for the other groups (except 'Very High') the value lies around 0.255 ± 0.006.

Currently we are assessing whether alternative approaches to traditional BCP metrics can be applied, which could take into account the influence of IPMs. This could include double Martin curve fitting (i.e. from the surface to the IPM, and downwards from the IPM) or alternative calculation of remineralization depth (i.e. not the depth at which 33% of the flux remains, but the depth at which this value does not increase again due

to IPMs). Such metrics suitable for IPMs would allow a quantitative evaluation of flux attenuation for profiles that do not follow a monotonous power-law decline with depth.

Main results achieved

In this work, we assessed the biological carbon pump using *in situ* imaging data from the UVP5. This global datasets greatly increases the data coverage of gravitational flux compared traditional sediment trap data, also providing a much higher vertical resolution.

Our findings demonstrate that the paradigm of monotonously decreasing particle flux with depth (following a power law function) does not hold true in many cases. Instead, many profiles display the prevalence of intermediate particle maxima (IPM), i.e. a renewed increase in particle abundance and flux in mesopelagic depths after initial decrease below the euphotic zone. Commonly used metrics for biological pump efficiency (Martin's b, remineralization length scale, and transfer efficiency) do not account for the presence of IPMs and may therefore yield distorted results.

Contribution to the overall objectives and relevant (KPIs)

WP3 and deliverable 3.2 contribute to ST1, 2 and 3, as well as O2.

WP3 and deliverable 3.2 contribute to KPIs 1, 2, 3, 6, 8 and 11, and may additionally contribute to KPIs 12-21 depending on involvement of partners with international efforts such as IPCC, WOA etc.

Impact and progress beyond state of the art

Our analysis does not display an influence of key environmental drivers (temperature, pH, oxygen) on particle flux attenuation. This contradicts theoretical expectations and earlier studies that suggested at least an effect of temperature on flux attenuation. This suggests that natural variability of particle fluxes due to other processes obscure the potential influence of environmental factors on biological processes involved in flux attenuation (e.g. bacterial degradation or zooplankton flux feeding).

Lessons learnt and links built

Not applicable

References

Bianchi, D., & Clements, D. (2023). Global reconstructions of particle biovolume, size distribution, and carbon export flux from the seasonal euphotic zone and maximum winter time mixed layer from particle profiles conducted during cruises from 2008 to 2020. https://hdl.handle.net/1912/29686

Clements, D. J., Yang, S., Weber, T., McDonnell, A. M. P., Kiko, R., Stemmann, L., & Bianchi, D. (2023). New Estimate of Organic Carbon Export From Optical Measurements Reveals the Role of Particle Size Distribution and Export Horizon. Global Biogeochemical Cycles, 37(3), e2022GB007633. https://doi.org/10.1029/2022GB007633

European Union-Copernicus Marine Service. (2018). Global ocean biogeochemistry hindcast [Dataset]. Mercator Ocean International. https://doi.org/10.48670/MOI-00019

Garcia, H. E., Wang, Z., Bouchard, C., Cross, S. L., Paver, C. R., Reagan, J. R., Boyer, T. P., Locarnini, R. A., Mishonov, A. V., Baranova, O. K., Seidov, D., & Dukhovskoy, D. (2024). World Ocean Atlas 2023, Volume 3: Dissolved Oxygen, Apparent Oxygen Utilization, and Dissolved Oxygen Saturation. https://doi.org/10.25923/RB67-NS53

GEBCO Bathymetric Compilation Group 2023. (2023). The GEBCO_2023 Grid—A continuous terrain model of the global oceans and land. (Version 1) [Documents,Network Common Data Form]. NERC EDS British Oceanographic Data Centre NOC. https://doi.org/10.5285/F98B053B-0CBC-6C23-E053-6C86ABC0AF7B

Key, R. M., Olsen, A., Lauvset, S. K., Velo, A., Lin, X., Schirnick, C., Kozyr, A., Tanhua, T., Hoppema, M., Jutterström, S., Steinfeldt, R., Jeansson, E., Ishii, M., Pérez, F. F., & Suzuki, T. (2015). Global Ocean Data Analysis Project, Version 2 (GLODAPv2) [Dataset]. https://doi.org/10.3334/CDIAC/OTG.NDP093_GLODAPV2

Kiko, R., Picheral, M., Antoine, D., Babin, M., Berline, L., Biard, T., Boss, E., Brandt, P., Carlotti, F., Christiansen, S., Coppola, L., De La Cruz, L., Diamond-Riquier, E., Durrieu De Madron, X., Elineau, A., Gorsky, G., Guidi, L., Hauss, H., Irisson, J.-O., … Stemmann, L. (2022). A global marine particle size distribution dataset obtained with the Underwater Vision Profiler 5. Earth System Science Data, 14(9), 4315–4337. https://doi.org/10.5194/essd-14-4315-2022

Locarnini, R. A., Mishonov, A. V., Baranova, O. K., Reagan, J. R., Boyer, T. P., Seidov, D., Wang, Z., Garcia, H. E., Bouchard, C., Cross, S. L., Paver, C. R., & Dukhovskoy, D. (2024). World Ocean Atlas 2023, Volume 1: Temperature. https://doi.org/10.25923/54BH-1613

Longhurst, A. (2007). Ecological Geography of the Sea. https://doi.org/10.1016/B978-0-12-455521-1.X5000-1

Martin, J. H., Knauer, G. A., Karl, D. M., & Broenkow, W. W. (1987). VERTEX: Carbon cycling in the northeast Pacific. Deep Sea Research Part A. Oceanographic Research Papers, 34(2), 267–285. https://doi.org/10.1016/0198-0149(87)90086-0

Mouw, C. B., Barnett, A., McKinley, G. A., Gloege, L., & Pilcher, D. (2016). Global ocean flux rates [Dataset]. In In supplement to: Mouw, CB et al. (2016): Global ocean particulate organic carbon flux merged with satellite parameters. Earth System Science Data, 8(2), 531-541, https://doi.org/10.5194/essd-8-531-2016. PANGAEA. https://doi.org/10.1594/PANGAEA.855594

Olsen, A., Key, R. M., Van Heuven, S., Lauvset, S. K., Velo, A., Lin, X., Schirnick, C., Kozyr, A., Tanhua, T., Hoppema, M., Jutterström, S., Steinfeldt, R., Jeansson, E., Ishii, M., Pérez, F. F., & Suzuki, T. (2016). The Global Ocean Data Analysis Project version 2 (GLODAPv2) – an internallyconsistent data product

for the world ocean. Earth System Science Data, 8(2), 297–323. https://doi.org/10.5194/essd-8-297-2016

Reygondeau, G., Longhurst, A., Martinez, E., Beaugrand, G., Antoine, D., & Maury, O. (2013). Dynamic biogeochemical provinces in the global ocean. Global Biogeochemical Cycles, 27(4), 1046–1058. https://doi.org/10.1002/gbc.20089